Journal of Nuclear Materials 397 (2010) 61–68

Contents lists available at ScienceDirect

Journal of Nuclear Materials

journal homepage: www.elsevier.com/locate/jnucmat

The kinetics of hydrogen desorption from and adsorption on zirconium hydride

K.A. Terrani [a,*], M. Balooch [a], D. Wongsawaeng [b], S. Jaiyen [b], D.R. Olander [a]

[a] Department of Nuclear Engineering, University of California, Berkeley, CA 94720-1730, USA
[b] Nuclear Technology Department, Chulalongkorn University, Bangkok 10330, Thailand

ARTICLE INFO

Article history:
Received 13 October 2009
Accepted 11 December 2009

ABSTRACT

Three sets of independent experiments were conducted to determine the kinetics of hydrogen desorption from and adsorption on δ-zirconium hydrides. One method involved measurement of hydrogen gas pressure-buildup as a result of dehydriding in a closed vessel. The other two involved thermogravimetric experiments, measuring the rate of mass loss during dehydriding under vacuum. Zeroth-order desorption and first order (with respect to gas-phase hydrogen) adsorption kinetics was determined. The Arrhenius dependence of rate constants showed excellent agreement among different experimental data. The activation energies for desorption and adsorption processes were determined as 205 ± 8 and 86 ± 15 kJ mol^{-1} respectively.

1. Introduction

Hydrogen-based nuclear fuels have been utilized in numerous occasions, particularly in the SNAP program [1] and as fuel for TRIGA research reactors. The advantages over oxide fuel for LWRs have been extensively documented (NED issue [2]). Briefly, hydrogen bound in the fuel acts as a neutron moderator augmenting the coolant for this purpose, permitting more compact core designs with higher power density. The prompt negative fuel–temperature reactivity feedback (long exploited in pulsing TRIGA reactors) renders control-rod ejection a benign event in LWRs (except at high burnups). From a materials perspective, hydride fuel has a 5-fold higher thermal conductivity than oxide fuel, resulting in operating temperatures low enough (<650 °C) even at high linear heat rates (40 kW/m) to avoid fission-gas release and to reduce stored energy. However, the rate of fission-product swelling is three times larger than that of oxide fuel.

Hydride fuel is produced by contacting U–Zr alloys (~45 wt.% U) with hydrogen gas at high temperature. Other alloy compositions containing thorium or minor actinides are also possible hydride fuels. In case of the U–Zr hydride fuel, controlling the hydrogen pressure during fabrication establishes the H/Zr ratio (typically 1.6). The resulting microstructure consists of micron-size metallic uranium particles dispersed in a matrix of zirconium hydride. The Zr–H phase diagram is well-established, as is the equilibrium hydrogen pressure as a function of temperature and H/Zr ratio (Eq. (1)) [3]. In Eq. (1), C is the hydrogen to zirconium ratio.

$$p_{H_2\text{-eq}}\ [\text{MPa}] = \left(\frac{C}{2-C}\right)^2 \exp\left(5.72 + 5.21C - \frac{172\ [\text{kJ mol}^{-1}]}{RT\ [\text{K}]}\right) \quad (1)$$

Fig. 1 indicates that substantial hydrogen pressures can be generated if the fuel is driven to high temperatures (>~800 °C) in a transient [5]. This in turn can release H_2 to the gap and the plenum, with several adverse consequences: (i) overpressurization of the fuel rod; (ii) permeation of hydrogen through the cladding (Zircaloy); (iii) hydrogen embrittlement of the cladding. Although the thermodynamic driving force for hydrogen loss from the zirconium hydride matrix in the fuel at high temperature exists, the kinetics of the process is unknown. The purpose of the present work is to report the results of several experiments bearing on the kinetics of the dehydriding process. All the results presented here pertain to the cubic δ-$ZrH_{1.6\pm x}$ phase [6].

2. Experimental setups

Three independent experiments yielding information on the dehydriding process were conducted. The first method involved measurement of hydrogen gas pressure-buildup in a closed vessel as the dehydriding reaction proceeded. The other two experiments, although independent, were conducted using thermogravimetric analysis (TGA) setups, measuring the rate of mass loss while dehydriding took place.

* Corresponding author. Address: Department of Nuclear Engineering, University of California, 4155 Etcheverry Hall, Berkeley, CA 94720-1730, USA. Tel.: +1 510 642 4077; fax: +1 510 643 9685.
E-mail address: terrani@berkeley.edu (K.A. Terrani).

0022-3115/$ - see front matter © 2009 Elsevier B.V. All rights reserved.
doi:10.1016/j.jnucmat.2009.12.008

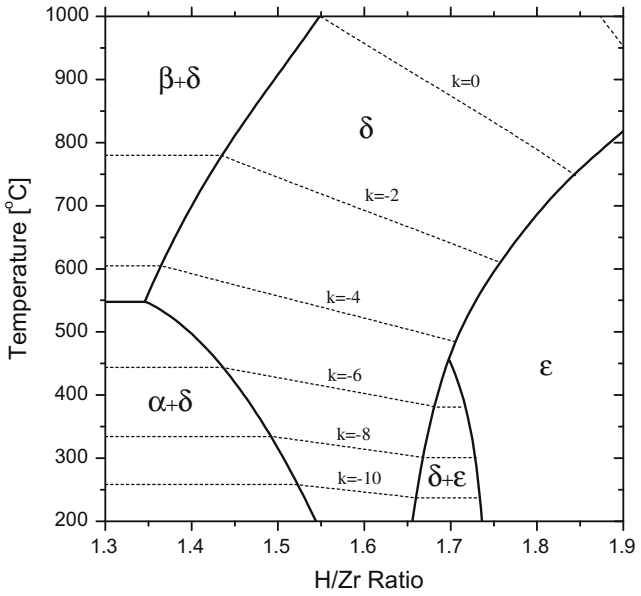

Fig. 1. Phase diagram for zirconium–hydrogen system [4] with equilibrium H_2 isobars labeled as $p_{H_2} = 10^k$ (MPa).

2.1. Pressure-buildup experiments

The rate of pressure increase inside a closed system due to dehydriding of zirconium hydride was measured in the experimental setup shown in Fig. 2.

A small disk of 99.9% purity zirconium metal (1.0 mm thick, 13.5 mm diameter) was initially cleaned by mechanical polishing and alcohol rinsing. The specimen was placed inside a 316 stainless-steel vessel that was then welded shut. After attaching a pressure transducer and a valve leading to a gas/vacuum management system, the vessel was placed in a furnace. The initial step in the experiment involved in situ production of hydride from the metal disk. The zirconium disk was heated to 750–920 °C in an H_2 atmosphere. The stoichiometry was controlled according to Eq. (1) by adjustment of the temperature and pressure. Upon hydriding the accompanied volume expansion increased the dimensions of the specimen by ~4%.

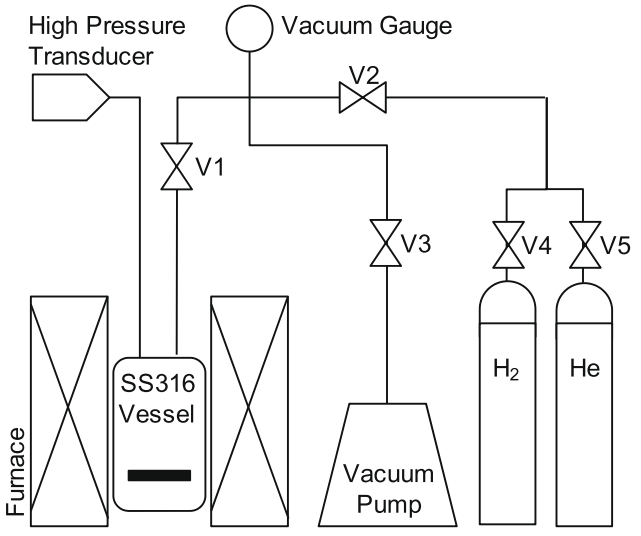

Fig. 2. Experimental setup for pressure-buildup measurements.

The sample initially underwent hydriding at 881 °C under 0.34 MPa of hydrogen gas pressure for duration of an hour. After any subsequent dehydriding step, the duration of hydriding at a different temperature was established by a rough diffusion analysis. The length of the hydrogen diffusion path is the half-thickness of the specimen ($l/2$). The diffusion coefficient of hydrogen in the δ-zirconium hydride reported by Majer et al. [7] is 2.1×10^{-10} m^2 s^{-1} at 800 °C and 3.7×10^{-10} m^2 s^{-1} at 900 °C. The characteristic diffusion time, defined as l^2/D, at these two temperatures is 20 and 11 min, respectively. Similar calculations were used to process hydrides of uniform hydrogen concentration at each temperature. The final dimensions of the hydride disks were 1.04 mm in thickness and 14.0 mm in diameter.

After the uniform hydriding was achieved across the sample, the system was quickly pumped down to vacuum and then isolated by valving off the vessel. Subsequently, the rise in pressure from vacuum due to dehydriding was monitored by a high-pressure transducer connected to the vessel. The volume of the vessel and the connecting tubing up to valve V1 and the interior of the pressure transducer was 1.95×10^{-5} m^3. The system was designed with minimal volume in order to achieve accurate pressure-change measurements. Hydriding and dehydriding were performed in sequence at constant temperature.

A minor complication with this technique is the permeability of stainless-steel to hydrogen. The leakage rate of hydrogen from the vessel can be written in terms of the parameters shown in Eq. (2), where Φ_o and H_Φ are the pre-exponential and activation energy of the permeation process, respectively.

$$R_{\text{leak}} = \Phi_o \frac{1}{\delta} \sqrt{p} \exp\left(\frac{-H_\Phi}{RT}\right) \tag{2}$$

δ is the thickness of the vessel wall. Permeation of hydrogen through stainless-steel has been extensively studied [8] and the activation energy is reported as 60 kJ mol^{-1}. The permeation rate was determined from the rate of pressure drop, using a vessel filled with hydrogen gas but no hydride specimen at different temperatures. The pre-exponential term and activation energy were determined as 1.1×10^{-4} mol H_2 m^{-1} s^{-1} MPa$^{-½}$ and 53 kJ mol^{-1}, respectively. As shown in Fig. 3, these results are in good agreement with literature values.

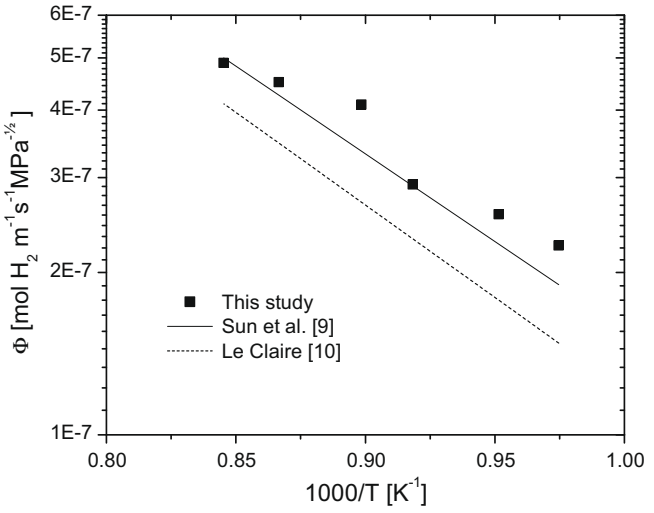

Fig. 3. Leakage rate of hydrogen (permeation) from the stainless-steel vessel as a function of temperature [9,10].

2.2. Thermogravimetric experiments

Two separate TGA experiments were conducted, one at Univ. of California, Berkeley California [11] (on zirconium samples) and another at Chulalongkorn Univ., Bangkok, Thailand (on Zircaloy specimens). In both cases a microbalance was utilized to measure changes in sample weight as a function of time.

The samples for the Berkeley experiment were initially polished and pickled in a solution of 50 vol.% water, 45 vol.% 16 M nitric acid and 5 vol.% 28 M hydrofluoric acid for 2 min. Specimens were then hung using a tungsten–rhenium wire into a quartz tube with controlled atmosphere, where temperatures up to 810 °C were attainable. The samples were first heated under vacuum then hydrided in a hydrogen atmosphere. The pre-dehydriding H/Zr ratio was fixed by controlling the temperature and hydrogen gas pressure, and was verified by the mass gain. Then, while at constant temperature, a vacuum on the order of 10^{-3} Pa was induced and maintained inside the quartz tube. The rate of hydrogen desorption was determined by measuring the weight-loss rate.

The second set of thermogravimetric experiments was performed using hydrided Zircaloy-2 tubes under similar conditions and experimental procedures.

Table 1
Experimental conditions and details.

Temperature (°C)	Pre-dehydriding		Post-dehydriding	
	H_2 pressure (MPa)	H/Zr ratio	H_2 pressure (MPa)	H/Zr ratio
743	0.042	1.632	0.016	1.546
770	0.092	1.654	0.039	1.579
798	0.294	1.704	0.066	1.581
800	0.464	1.735	0.075	1.589
829	0.222	1.639	0.083	1.553
830	0.454	1.694	0.091	1.560
852	0.412	1.658	0.118	1.550
859	0.147	1.560	0.089	1.512
863	0.433	1.648	0.124	1.538
880	0.457	1.630	0.137	1.522
881	0.341	1.603	0.142	1.524
902	0.447	1.599	0.166	1.508
920	0.457	1.578	0.217	1.508

3. Results and analysis

3.1. Pressure-buildup experiments

A typical graph showing the rise in pressure as a function of time for the first 6 min during dehydriding is presented in Fig. 4. The rise in pressure takes place rapidly and reaches equilibrium conditions in a matter of minutes. Experiments were performed at 13 different temperatures and starting H/Zr ratios (Table 1). Pre and post-dehydriding hydrogen gas pressures are given in Table 1. The H/Zr ratios were calculated by substituting the steady-state hydrogen pressures into Eq. (1).

Conservation of mass at the surface of the hydride disk requires that the net rate of H_2 desorption equalsthe hydrogen atom flux to the surface by diffusion (Eq. (3)). The term taking into account the change in the hydrogen stored at the surface layer is ignored since it is many orders of magnitudes smaller. The rate of hydrogen gas accumulation inside the vessel is due to H_2 adsorption and desorption from the hydride and to the rate at which the hydrogen leaks from the vessel (Eq. (4) and Fig. 5).

$$\frac{1}{2}R_{\mathrm{diff}}|_{x=l/2} = R_{\mathrm{des}} - R_{\mathrm{ads}} \tag{3}$$

$$\frac{V}{RT}\frac{dp}{dt} = (R_{\mathrm{des}} - R_{\mathrm{ads}})S_d - \frac{1}{2}R_{\mathrm{leak}}S_v \tag{4}$$

The diffusion and leakage terms in the above equations are divided by a factor of 2 since they correspond to flux of hydrogen atoms and the rates of adsorption and desorption correspond to that of hydrogen gas. V, R, T, S_d, and S_v are vessel volume (1.95×10^{-5} m^3), gas constant, temperature, disk surface area (3.56×10^{-4} m^2), and vessel surface area ($\sim 1.6 \times 10^{-3}$ m^2), respectively. The left hand side of Eq. (4) is experimentally measured. The leakage term is also known since it was measured in Section 2.1. At each time, the slope dp/dt was read from the curves in Fig. 4 and input to Eq. (5). Subsequently the flux (net rate of desorption) at the hydride surface as a function of time, corrected for hydrogen leakage from the vessel, could be calculated using experimental data. Keep in mind that the actual pressures measured as a function of time (not corrected for leakage)

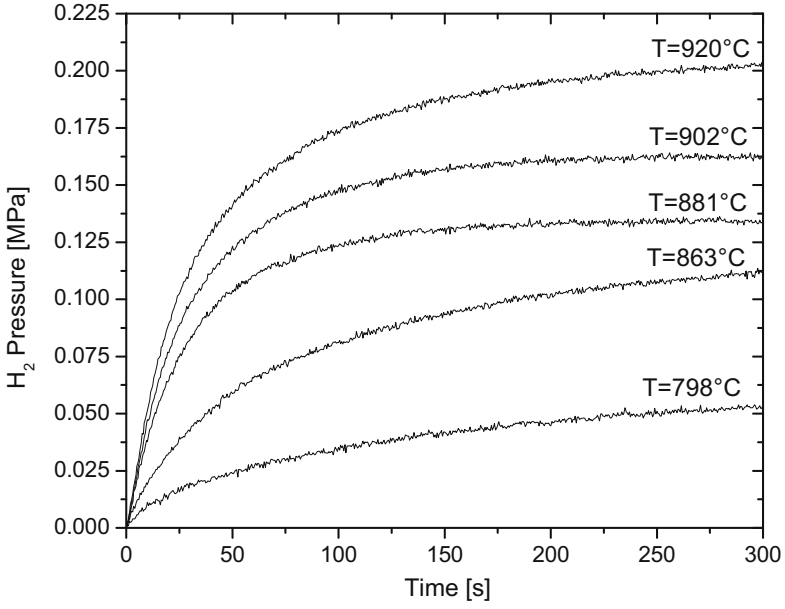

Fig. 4. Typical results corresponding to accumulation of hydrogen gas inside the vessel as a function of time.

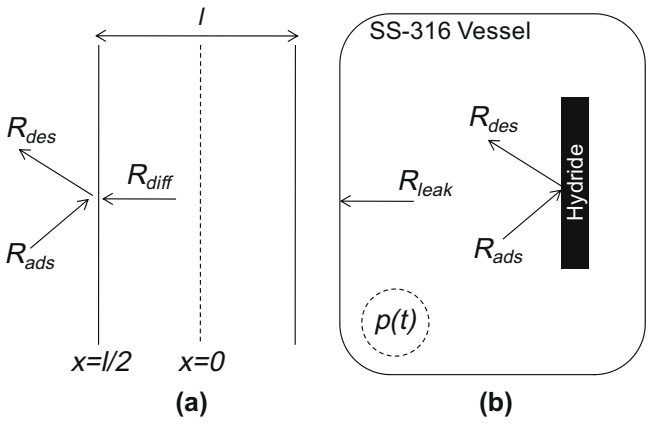

Fig. 5. Conservation of hydrogen (a) at the hydride surface (b) inside the vessel.

were input to R_{leak} since they represent what is physically experienced by the sample.

$$J_{des} = \frac{1}{S_d}\left(\frac{V}{RT}\frac{dp}{dt} + \frac{1}{2}R_{leak}S_v\right) \quad (5)$$

Fig. 6 shows the net rate of hydrogen desorption from the surface as a function of hydrogen gas pressure (rather than time). The linearity of these plots indicates that the H_2 desorption flux can be described by an equation of the form:

$$J_{des} = K(p_{eq} - p) \quad (6)$$

where p_{eq} is the equilibrium pressure (Fig. 4, $t > 300$ s) and K is a constant.

3.2. Thermogravimetric experiments

A typical graph showing the change in the hydride content as function of time during the TGA (thermogravimetric analysis) is shown in Fig. 7 for the experiments performed on zirconium samples. The rate of mass loss is constant over a considerable extent of the δ-$ZrH_{1.6\pm x}$ region. Very similar results with linear mass loss behavior were observed in the Zircaloy TGA experiments.

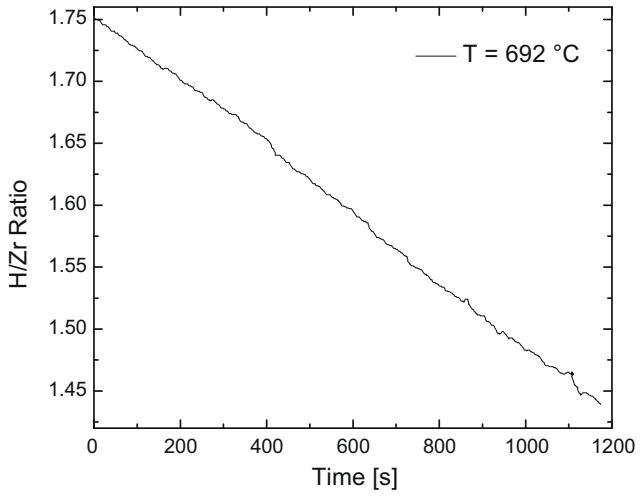

Fig. 7. Reduction of the H/Zr ratio determined from mass loss of hydrided zirconium at 692 °C.

3.3. Analysis of the experimental data

The surface reaction obeys zeroth-order kinetics, as in no influence of surface concentration on the rates of adsorption and desorption is observed. Figs. 6 and 7 clearly show concentration independent rate constants for both the desorption and adsorption processes. Inapplicability of second order surface kinetics and the evidence of change in surface hydrogen concentration during the dehydriding process is discussed in Appendix A. Appendix B outlines the steps taken to investigate the possibility of bulk diffusion limited kinetics and its invalidity for this case. The lack of dependence of the rate of mass loss on the H/Zr ratio is a characteristic of a zeroth-order desorption process. When coupled to an adsorption step that obeys first-order kinetics, the net desorption flux is expressed by:

$$J_{des} = R_{des} - R_{ads} = k_{des} - k_{ads}p \quad (7)$$

Eq. (7) has the same form as Eq. (6), from which the rate constants are identified as:

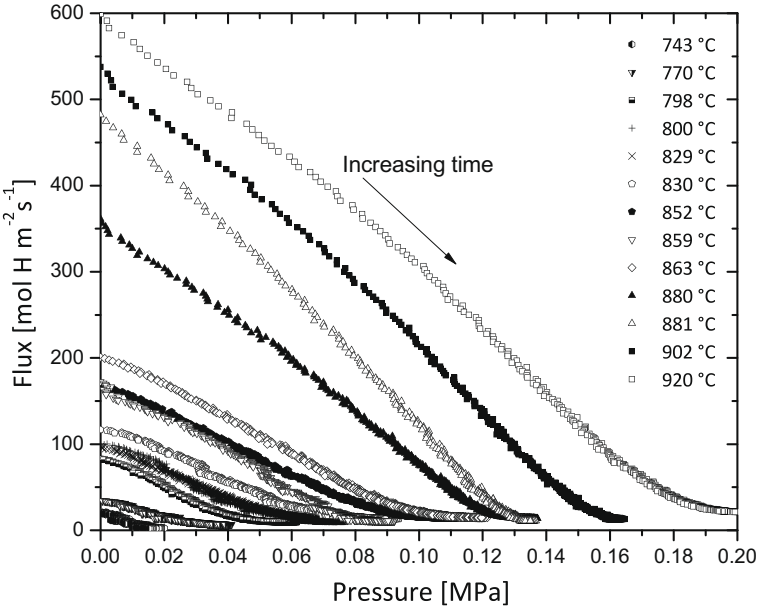

Fig. 6. Evolution of the net hydrogen flux versus hydrogen gas pressure in the vessel during the dehydriding process.

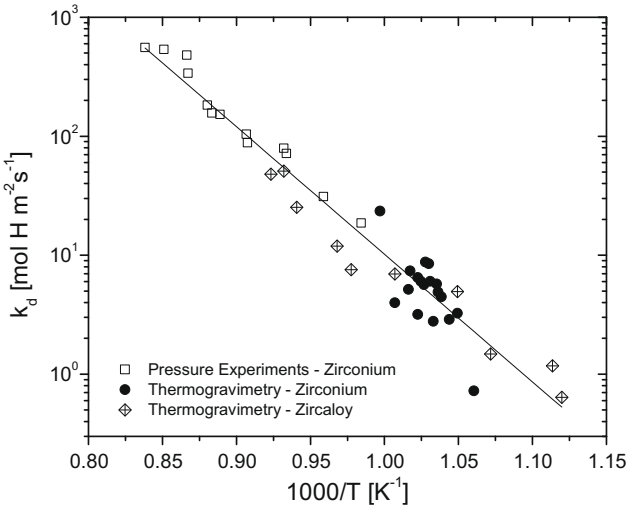

Fig. 8. Arrhenius dependence of the desorption rate constant.

$$k_{des} = Kp_{eq}, \quad k_{ads} = K \tag{8}$$

The K values obtained from linear fits to the lines in Fig. 6 provide the two rate constants as functions of temperature. In Fig. 8, the desorption rate constants from all three experiments (pressure-buildup, two TGA) are plotted in Arrhenius fashion where the agreement among the three data sets is excellent. The desorption rate constant was determined through a linear fit and is presented along with the standard error in regression as:

$$k_{des}\ [\text{mol H m}^{-2}\text{s}^{-1}] = \exp\left(27.0 \pm 0.9 + \frac{-205 \pm 8\ [\text{kJ mol}^{-1}]}{RT\ [\text{K}]}\right) \tag{9}$$

where the activation energy is in kJ mol^{-1} and T is in Kelvin. Based on the pressure-buildup data, Fig. 9 depicts the adsorption rate constant as a function of temperature where k_{ads} is expressed by:

$$k_{ads}\ [\text{mol H m}^{-2}\text{s}^{-1}\text{MPa}^{-1}] = \exp\left(16.7 \pm 1.6 + \frac{-86 \pm 15\ [\text{kJ mol}^{-1}]}{RT\ [\text{K}]}\right) \tag{10}$$

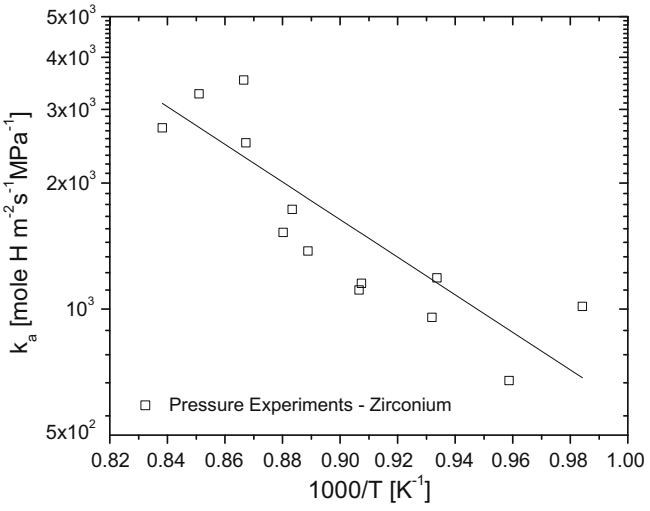

Fig. 9. Arrhenius dependence of the adsorption rate constant determined from the pressure-buildup experiments.

4. Discussion

Zeroth-order desorption kinetics is rare, but not unknown. Bienfait and Venables have reported this behavior for xenon adsorbed on 0001 graphite planes [12]. The same order kinetics has been reported for desorption of O_2 from oxide films on tungsten [13]. In both cases desorption leaves behind an identical layer of the material (adsorbate in case of xenon and substrate in case of tungsten oxide). However, the current system is different because the desorbing gas is supplied to the surface by diffusion in the substrate solid. Throughout the dehydriding process the hydrogen concentration in the bulk, which feeds the surface hydrogen, is constantly reduced.

A more relevant system is hydrogen on nickel and iron films, for which zeroth-order desorption kinetics was observed [14,15]. This behavior was attributed to a precursor state of molecular hydrogen on the surface that ultimately controls the desorption rate. However, the applicability of this mechanism to the current system is questionable. The activation energy of 205 kJ mol^{-1} is much larger than the values reported in the mentioned studies (~25 kJ mol^{-1}) for a hydrogen molecule in a precursor state on the surface to overcome the barrier to desorption. A more likely rate-controlling step is the recombination of H atoms on the surface to form H_2, a step that requires rupture of zirconium–hydrogen bonds. Enthalpy of formation of zirconium hydride has been reported as 160 kJ mol^{-1} through calorimetric experiments [16]; the magnitude of which is coherent with the measured activation energy for desorption. For this mechanism to exhibit zeroth-order kinetics, the atomic adsorption sites at the surface need to be saturated. High concentration of hydrogen atoms in the bulk along with their significant mobility at high temperatures make it plausible to assume saturation of the surface sites during hydrogen desorption. Consequently this implies that the bulk-to-surface, and gas-to-surface transfer processes are fast, and the overall process is bottlenecked by the surface-recombination step. This mechanism permits establishment of a constant atomic hydrogen concentration on the surface even in the presence of desorption as H_2.

Yet the above mechanism cannot hold throughout the entire process, since ultimately thermodynamic equilibrium relationship between the hydrogen gas and the hydride presented in Eq. (1) is violated. At equilibrium the rates of desorption and adsorption are equal and therefore the net flux at the surface is zero. Setting $k_{des} = -k_{ads}\, p_{eq}$ at equilibrium we can derive the equilibrium pressure as:

$$p_{eq}\ [\text{MPa}] = 3.0 \times 10^4 \exp\left(\frac{-119\ [\text{kJ mol}^{-1}]}{RT\ [\text{K}]}\right) \tag{11}$$

Eq. (11), derived from the kinetic data, is compared to the equilibrium hydrogen pressure from Eq. (1) in Fig. 10.

A possible explanation for the difference between the two lines is the failure of the zeroth-order kinetic model as equilibrium is approached. Therefore the rate limiting step at conditions close to equilibrium conditions described in Eq. (1) is unknown and its dependence on hydrogen concentration does not obey the zeroth-order kinetics.

5. Conclusions

Dehydriding of zirconium hydride has been studied in three experimental apparatuses: a pressure-buildup procedure in a closed vessel and two TGAs. The kinetic data from all three tests showed zeroth-order desorption kinetics. This was attributed to slow surface H atom recombination in conjunction with rapid resupply of the surface from the hydrogen in the solid hydride. The adsorption step was found to be first order with respect to gas-phase hydrogen. The proposed model predicted the dehydriding

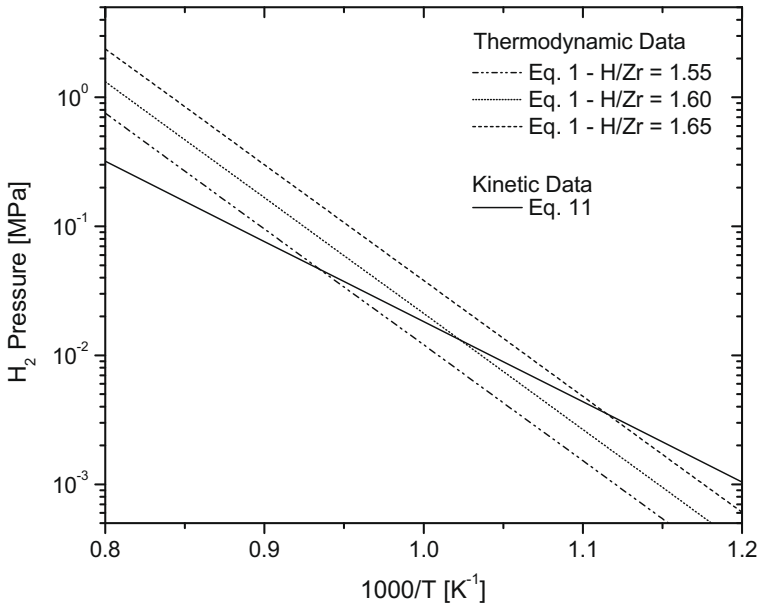

Fig. 10. Comparison of the equilibrium hydrogen pressure over $ZrH_{1.6}$ from thermodynamic measurements with that inferred from the present kinetic data.

kinetics over a wide range of conditions, but failed as equilibrium was approached.

Appendix A

A.1. Inapplicability of second order surface kinetics

Langmuir [17] initially proposed the simplified model describing the surface adsorption and desorption processes involved while gaseous species are adsorbed on solid surfaces. Since then the theory has developed and extended significantly to describe a much larger range of surface phenomenon [18]. In case of systems involving a diatomic gas and a solid the kinetics is generally dependent on the surface concentration of adsorbed species to the second order. Typical formulation of adsorption and desorption rates are shown in Eqs. (A1) and (A2). The pre-exponential term in the desorption rate is the product of the surface diffusivity of the adsorbed species, combinatorial number, and the aerial density of the total surface sites. In case of the adsorption rate the pre-exponential term is the product of the constants in the collision rate, the sticking probability constant, and the coordination number of the surface sites.

$$R_{\mathrm{des}} = k_d C^2 e^{\frac{-H_d}{RT}} \tag{A1}$$

$$R_{\mathrm{ads}} = k_a p_{\mathrm{H_2}} (1-C)^2 e^{\frac{-H_a}{RT}} \tag{A2}$$

In the above scenario, it is assumed that the hydrogen atom concentration in the bulk right beneath the surface and the adsorbed surface hydrogen concentration are in equilibrium. The net desorption, in case of surface reaction rate controlled through second order kinetics, is the difference between the two above equations. In Fig. 6 a linear relationship between the outgoing flux and hydrogen gas pressure is portrayed. To investigate the applicability of this model the evolution of surface hydrogen concentration during the dehydriding process needs to be known. By applying Fick's first law the rate of diffusion into the surface of the hydride is determined as:

$$R_{\mathrm{diff}}|_{x=l/2} = -2DN_{\mathrm{Zr}} \left.\frac{\partial C_s}{\partial x}\right|_{x=l/2} \tag{A3}$$

where N_{zr} is the zirconium number density in δ-zirconium hydride (the number density of hydrogen lattice sites is twice that of zirconium atoms, hence N_{zr} is multiplied by 2) and C_s is the surface H/Zr ratio. Substituting for the difference between rates of desorption and adsorption from Eqs. (3) and (A3) into (4), the following is formulated:

$$\left.\frac{\partial C_s}{\partial x}\right|_{x=l/2} = \frac{1}{-DN_{\mathrm{Zr}}}\left[\frac{V}{RTS_d}\frac{dp}{dt} + \frac{S_v}{2S_d}R_{\mathrm{leak}}\right] \tag{A4}$$

Eq. (A4), employing the experimental results, could serve as the boundary condition in order to solve the transient diffusion equation (Fick's second law) across the hydride disk during the dehydriding process. The disks are assumed to have uniform hydrogen concentration across the thickness at the beginning of the dehydriding process that is determined by the pressure at which the disks were processed (initial condition). The solution of diffusion equation (method discussed in Appendix C), using this boundary condition is shown for one of the samples in Fig. A1 in a contour plot where the magnitude of the H/Zr ratio across the half-thickness of the disk and as a function of time is depicted.

The evolution in the surface hydrogen concentration alongside the change in hydrogen gas pressure inside the vessel as a function of time is shown in Fig. A2.

The evolution in surface hydrogen concentration shown in Fig. A2 is such that it is not possible to predict the observed flux (as shown in Fig. 6) utilizing Eqs. (A1) and (A2). This underlines the inapplicability of second order surface kinetics to describe the desorption process during the pressure-buildup experiments. The TGA results also contradict the applicability of second order surface kinetics since no sign of concentration dependence on the desorption rate (the adsorption rate is negligible throughout the TGA experiment since the dehydriding is performed under vacuum) is present. During the TGA experiment the hydrogen concentration is continuously reduced across the hydride while the net desorption flux remains constant (Fig. 7).

Appendix B

B.1. Inapplicability of diffusion limited kinetics

In order to determine whether the desorption reaction is diffusion limited, the computed pressure-buildup scenarios of the diffusion limited case is compared to the experimental results. The

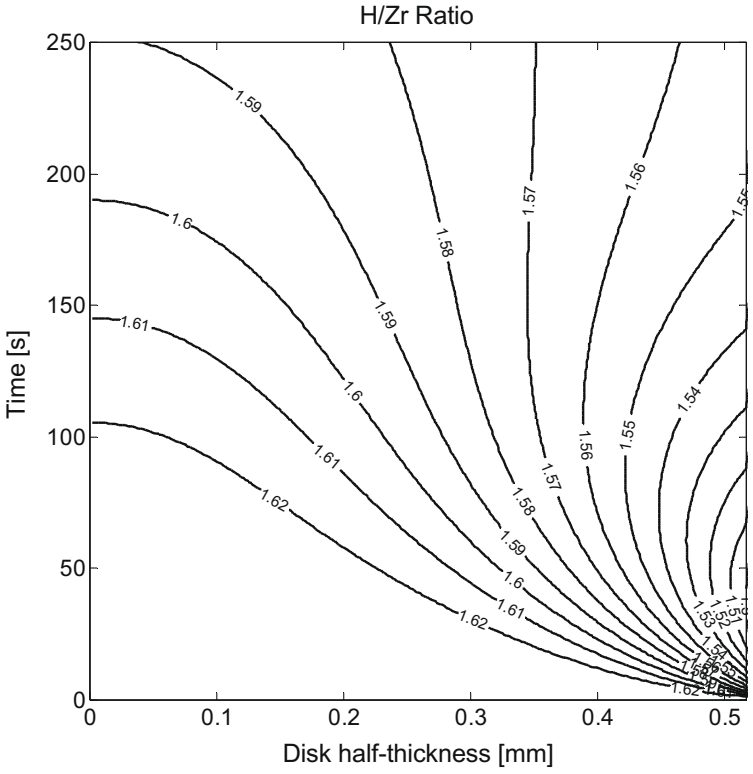

Fig. A1. Evolution of hydrogen concentration across the disk and as a function of time during dehydriding at 880 °C with initial uniform H/Zr ratio of 1.63.

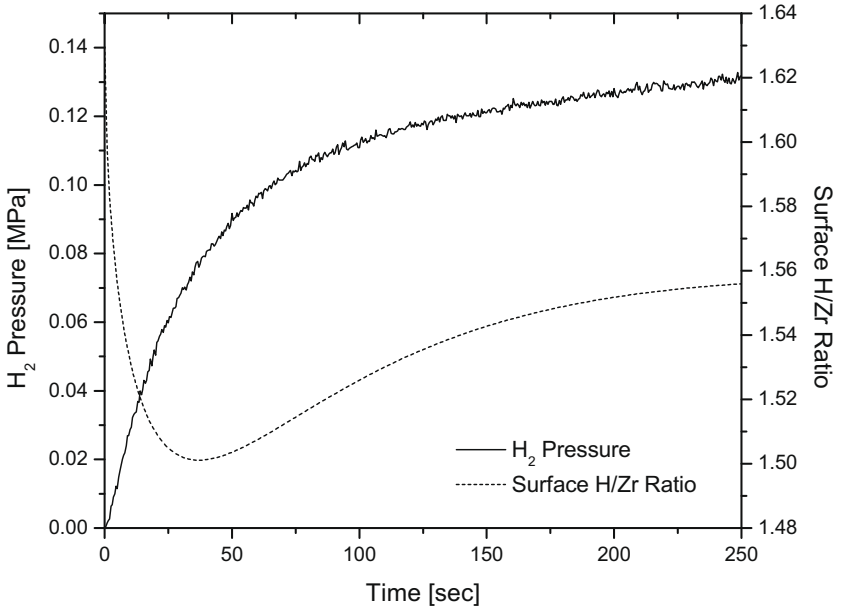

Fig. A2. Accumulation of hydrogen gas inside the vessel and change in H/Zr ratio at the surface of hydride as a function of time during dehydriding at 880 °C with initial uniform H/Zr ratio of 1.63.

computation assumes that the surface hydrogen concentration instantaneously becomes in equilibrium with the pressure inside the vessel according to Eq. (1). This provides the surface boundary condition to solve the diffusion equation. The initial condition assumes that the vessel gas pressure at the onset of the dehydriding process is approximately zero. The flux at the surface is then simply calculated using hydrogen concentration gradient at the surface during the dehydriding process (independent of the experimental results). The rate of change in vessel pressure could then be determined as shown in Eq. (B1). In the right hand side of the equation the leakage term and the concentration gradient at the surface are known through experimental data and solution to the diffusion equation respectively.

$$\frac{dp}{dt} = \frac{RTS_d}{V}\left[-DN_{Zr}\left.\frac{\partial C_s}{\partial x}\right|_{x=l/2} - \frac{S_v}{2S_d}R_{leak}\right] \tag{B1}$$

The solution scheme for the one-dimensional diffusion equation, generally applicable to this case, is discussed in Appendix C. The computed pressure-buildup results of the diffusion limited case deviate significantly from experimental results in two ways. The initial flux from the surface is orders of magnitude larger than what is determined experimentally in Section 3.1 and also the equilibrium hydrogen pressure at the end of the desorption process is largely under and overestimated at high and low temperatures respectively.

Also considering the TGA results, in case of diffusion limited kinetics it is logical to expect that the surface hydrogen concentration gradient (and therefore the dehydriding rate) decreases as a function of time. This is the case since the surface hydrogen concentration is fixed (by the constant vacuum induced at the surface) and the bulk concentration is continuously decreasing. However no such observation is apparent in Fig. 7 where the rate (the slope of the mass loss curve) is constant. Therefore the possibility of diffusion limited kinetics is ruled out.

Appendix C

C.1. Numerical solution to the one-dimensional diffusion equation

The one-dimensional diffusion equation is a linear partial differential equation (Eq. (C1)). Discretization of this equation is done utilizing the Crank and Nicolson scheme [19], in which time is discretized with the trapezoid rule and space with central difference. This first step is shown in Eq. (C2):

$$\frac{\partial C}{\partial t} = -D\nabla C \tag{C1}$$

$$\frac{1}{\Delta t}\left(C_i^{j+1} - C_i^j\right) = \frac{-D}{2\Delta x}\left[\left(\frac{\partial C}{\partial x}\right)_{i+1/2}^{j+1} - \left(\frac{\partial C}{\partial x}\right)_{i-1/2}^{j+1} + \left(\frac{\partial C}{\partial x}\right)_{i+1/2}^{j} - \left(\frac{\partial C}{\partial x}\right)_{i-1/2}^{j}\right] \tag{C2}$$

where i and j indicate the spatial node and time step, respectively. All terms are considered as node-centered. The equation is expanded and shuffled more:

$$C_i^{j+1} - C_i^j = \omega\left[C_{i+1}^{j+1} - 2C_i^{j+1} + C_{i-1}^{j+1} + C_{i+1}^{j} - 2C_i^j + C_{i-1}^j\right] \tag{C3}$$

$$\omega = \frac{-D\Delta t}{2\Delta x^2} \tag{C4}$$

The final form of the semi-implicitly discretized diffusion equation is acquired and a marching procedure is performed with time, solving for the $j+1$th iterate from the known jth iterate:

$$\begin{bmatrix} \omega+2 & -1 & 0 & 0 & 0 \\ -1 & \omega+2 & -1 & 0 & 0 \\ 0 & \ddots & \ddots & \ddots & 0 \\ 0 & 0 & -1 & \omega+2 & -1 \\ 0 & 0 & 0 & -1 & 1 \end{bmatrix} \begin{bmatrix} C_1^{j+1} \\ C_2^{j+1} \\ C_3^{j+1} \\ \vdots \\ C_N^{j+1} \end{bmatrix} = \begin{bmatrix} \omega-2 & 1 & 0 & 0 & 0 \\ 1 & \omega-2 & 1 & 0 & 0 \\ 0 & \ddots & \ddots & \ddots & 0 \\ 0 & 0 & 1 & \omega-2 & 1 \\ 0 & 0 & 0 & 1 & -1+\frac{\xi}{C_N^j} \end{bmatrix} \begin{bmatrix} C_1^j \\ C_2^j \\ C_3^j \\ \vdots \\ C_N^j \end{bmatrix} \tag{C5}$$

where ξ is the term incorporating the boundary condition. For instance in case of the boundary condition discussed in Eq. (A4) ξ is:

$$\xi = \frac{-2\Delta x}{DN_{Zr}S_d}\left(\frac{V}{RT}\frac{dp}{dt} + \frac{S_v}{2}R_{leak}\right) \tag{C6}$$

It needs to be specified that the diffusion coefficient is assumed constant over the range of different hydrogen concentrations in the hydride.

References

[1] N.F. Davies, R.E. Forrester, Effects of Irradiation on Hydrided Zirconium–Uranium Alloy NAA 120-4 Experiment, AI-AEC-12963, SNAP Program.
[2] Full issue, Nucl. Eng. Design. 239 (2009) 1373.
[3] W. Wang, D. Olander, J. Am. Ceram. Soc. 78 (1995) 3323.
[4] K. Moore, W. Young, J. Nucl. Mater. 27 (1968) 316.
[5] K.A. Terrani, J.E. Seifried, D.R. Olander, J. Nucl. Mater. 392 (2009) 192.
[6] R. Beck, Trans. Am. Soc. Met. 55 (1962) 555.
[7] G. Majer, W. Renz, R. Barnes, J. Phys.: Condens. Matter 6 (1994) 2935.
[8] C. San Marchi, B. Somerday, S. Robinson, Int. J. Hydrogen Energy 32 (2007) 100.
[9] X. Sun, J. Xu, Y. Li, Mater. Sci. Eng. A114 (1989) 179.
[10] A.D. LeClaire, Defect Diffus. Forum 34 (1983) 1.
[11] D.M. Gutowski, Kinetics of Hydrogen Uptake and Release from Zirconium Hydride, Master's Thesis, University of California, 2005.
[12] J.A. Venables, M. Bienfait, Surf. Sci. 61 (1970) 667.
[13] D.A. King, T. Madey, J.T. Yates, J. Chem. Phys. 55 (1971) 3247.
[14] M.R. Shanabarger, Solid State Commun. 14 (1974) 1015.
[15] M.R. Shanabarger, Surf. Sci. 150 (1985) 451.
[16] D.R. Fredrickson, R.L. Nuttall, H.E. Flotow, W.N. Hubbard, J. Phys. Chem. 67 (7) (1963) 1506.
[17] I. Langmuir, J. Am. Chem. Soc. 40 (1918) 1361.
[18] C. Bamford, C. Tipper, R. Compton, Comprehensive Chemical Kinetics: Simple Processes at the Gas–Solid Interface, vol. 19, 1979.
[19] J. Crank, P. Nicolson, Proc. Cambridge Philos. Soc. 43 (1947) 50.